

This is an Open Access document downloaded from ORCA, Cardiff University's institutional repository: <https://orca.cardiff.ac.uk/id/eprint/109827/>

This is the author's version of a work that was submitted to / accepted for publication.

Citation for final published version:

Li, Yuyin, Zhang, Yahui and Kennedy, David 2018. Reliability analysis of subsea pipelines under spatially varying ground motions by using subset simulation. *Reliability Engineering & System Safety* 172 , pp. 74-83. 10.1016/j.ress.2017.12.006

Publishers page: <http://dx.doi.org/10.1016/j.ress.2017.12.006>

Please note:

Changes made as a result of publishing processes such as copy-editing, formatting and page numbers may not be reflected in this version. For the definitive version of this publication, please refer to the published source. You are advised to consult the publisher's version if you wish to cite this paper.

This version is being made available in accordance with publisher policies. See <http://orca.cf.ac.uk/policies.html> for usage policies. Copyright and moral rights for publications made available in ORCA are retained by the copyright holders.



1 **Reliability Analysis of Subsea Pipelines under Spatially**
2 **Varying Ground Motions by Using Subset Simulation**

3

4 Yuyin Li^a, Yahui Zhang^{a*}, David Kennedy^b

5

6 ^a *State Key Laboratory of Structural Analysis for Industrial Equipment, Department of*

7 *Engineering Mechanics, International Center for Computational Mechanics, Dalian*

8 *University of Technology, Dalian 116023, PR China;*

9 ^b *School of Engineering, Cardiff University, Cardiff CF24 3AA, Wales, UK*

10

11 Corresponding author:

12 Dr. Y. H. Zhang

13 State Key Laboratory of Structural Analysis for Industrial Equipment, Department of

14 Engineering Mechanics, Dalian University of Technology, Dalian 116023, PR China

15 Email: zhangyh@dlut.edu.cn

16 Tel: +86 411 84706337

17 Fax: +86 411 84708393

18

19

20 **Abstract**

21 A computational framework is presented to calculate the reliability of subsea pipelines
22 subjected to a random earthquake. This framework takes full account of the physical
23 features of pipelines and the earthquake, and also retains high computing precision and
24 efficiency. The pipeline and the seabed are modelled as a Timoshenko beam and a Winkler
25 foundation, respectively, while the unilateral contact effect between them is considered.
26 The random earthquake is described by its power spectrum density function and its spatial
27 variation is considered. After suitable discretizations in the spatial domain by the finite
28 element method and the time domain by the Newmark integration method, the dynamic
29 unilateral contact problem is derived as a linear complementarity problem (LCP). Subset
30 Simulation (SS), which is an advanced Monte Carlo simulation approach, is used to
31 estimate the reliability of pipelines. By means of numerical examples, the accuracy and
32 robustness of SS are demonstrated by comparing with the direct Monte Carlo simulation
33 (DMCS). Then a sensitivity analysis of the reliability and a failure analysis are performed
34 to identify the influential system parameters. Finally, failure probabilities of subsea
35 pipelines are assessed for three typical cases, namely, with and without the unilateral
36 contact effect, with different grades of spatial variations and with different free spans. The
37 influences of these effects or parameters on the reliability are discussed qualitatively.

38 **Key words:** subsea pipeline; random earthquake; spatially varying ground motion;
39 unilateral contact; reliability; subset simulation

40 **1 Introduction**

41 Subsea pipelines always rest freely on the seabed, rather than being buried or
42 anchored. Due to the scouring or unevenness of the seabed, pipelines will not touch down
43 uniformly along the length of the pipe, and free spanning inevitably occurs. Since subsea
44 pipelines are generally important and costly facilities, their reliability has been a
45 fundamental problem of interest throughout the world. In recent years, attention has
46 mainly been focused on corrosion failure [1], vortex-induced vibration fatigue damage
47 [2], on-bottom lateral instability [3] and so on. As an occasional random excitation, a
48 strong earthquake poses a tremendous threat to the safety of pipelines, and hence the
49 dynamic response and reliability of pipelines under an earthquake have also received
50 great attention. However, the emphasis has been on buried pipelines, with much less
51 research on unburied pipelines. The relevant standards, such as DNV-OS-F101 [4], do
52 not provide design methods or guidelines for the earthquake reliability of unburied subsea
53 pipelines. The failure of structures under an earthquake is a typical first-excursion
54 problem. To assess the first-excursion reliability, the main difficulties arise from (1) the
55 solution of random responses of structures under the earthquake and (2) the evaluation of
56 the reliability by using the random responses obtained in (1).

57 In the solution of random responses, one of the most important problems is how to
58 consider the relationship between pipelines and seabed as exactly as possible. In the
59 literature on the dynamic analysis of unburied pipelines, pipelines are widely simplified

60 as multi-supported beams or beams on an elastic foundation [5-8]. However, in reality
61 unburied pipelines are constrained unilaterally by the seabed, which means that the
62 reaction of the seabed can only be compressive, but not tensile. Hence, during the
63 vibration of pipelines, particularly when the deformation takes place predominantly in the
64 vertical plane, a separation of pipelines and the seabed will occur. Clearly, both the multi-
65 supported beam model and the elastic foundation beam model will overestimate the
66 constraint between pipelines and the seabed, and neither of these two models can take the
67 separation of pipelines and the seabed into consideration. Therefore, a unilateral contact
68 model is more appropriate to simulate the relationship between unburied pipelines and
69 the seabed, and such models have been applied to various kinds of static and dynamic
70 analysis of the subsea pipelines, such as the elastic and elasto-plastic analysis of subsea
71 pipelines subjected to vertical static loads [9], stress analysis problems involving subsea
72 pipelines freely resting upon irregular seabed profiles [10], optimal control of the dynamic
73 response of subsea cables constrained by a frictionless rigid seabed [11] and so on.
74 Nevertheless, due to the contact nonlinearity, obtaining the dynamic response of a
75 unilateral contact system is a challenging task, and some classical methods of structural
76 analysis, such as the analytical method used in [6] or the frequency-domain method used
77 in [8], are no longer feasible. As a consequence, the unilateral model is not used
78 frequently for the dynamic analysis of subsea pipelines under an earthquake, despite its
79 good approximation to the relationship between subsea pipelines and the seabed. In

80 general, the unilateral contact problem is dealt with by numerical methods, e.g., the
81 combination of the finite element method and step-by-step integration method. In each
82 time step, the nonlinear problem is solved by the Newton-Raphson method or a similar
83 iterative method [10]. The unilateral contact problem can also be treated by deriving it as
84 a linear complementary problem (LCP). There are many well-developed methods to solve
85 the LCP and most of them have been included in commercial software, making it much
86 more convenient to solve the unilateral contact method by the LCP method than Newton-
87 Raphson methods.

88 The earthquake excitation model is another key point in the process of the solution
89 of random responses of subsea pipelines. Due to the natural random factors of the soil,
90 the motion of the seabed is more likely to exhibit strong randomness during an earthquake,
91 as are the responses of structures. Hence it is more rational to study the responses of
92 structures subjected to an earthquake from the point of view of the random vibration. On
93 the other hand, variations can be found during earthquake wave propagation along the
94 length of long-span structures, such as subsea pipelines, which result in differences in the
95 amplitude and phase of ground motions at the supports of the structures. This
96 phenomenon is termed as spatially varying ground motions [13]. Many random vibration
97 methods have been developed for the analysis of multi-span structures subjected to
98 spatially varying ground motions [14-16]. However, these methods are no longer feasible
99 after taking the contact of pipelines and the seabed into consideration, for two reasons.

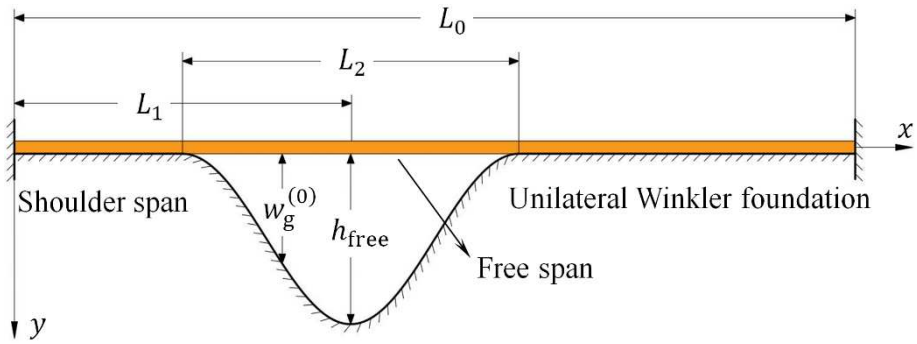
100 Firstly, these methods are based on the power spectrum density or response spectrum,
101 which are essentially frequency-domain methods, and thus cannot be used to treat the
102 contact problem because of the nonlinearity. Secondly, the response of a nonlinear system
103 is always non-Gaussian even if the input is a Gaussian random process, and these methods
104 can only provide the first- and second-order statistical moments of the response, which
105 are insufficient to describe totally the statistical properties of the non-Gaussian response.
106 In the circumstances, the Monte Carlo simulation (MCS) method, which is suitable for
107 both linear and nonlinear random vibration analysis, seems to be the best and only choice,
108 despite its relatively large computational requirements [17].

109 After obtaining the random response of subsea pipelines, the problem which follows
110 is how to estimate the reliability of subsea pipelines through this random response. Due
111 to the complex nature of the first-excursion failure and the unilateral contact problem, the
112 limit state function of subsea pipelines is extremely complicated and has no explicit
113 expression, while extreme values of the random response are not Gaussian distributed.
114 Therefore, popular methods of reliability analysis such as the first order reliability method
115 (FORM) [18], second order reliability method (SORM) [19], point estimate method
116 (PEM) [20], etc. are unable to predict accurately the reliability of subsea pipelines under
117 an earthquake. The MCS is one of most well-known methods for reliability analysis
118 because it is independent of the complexity and dimension of the problem. However, the
119 number of samples required by the MCS is proportional to the reciprocal of the failure

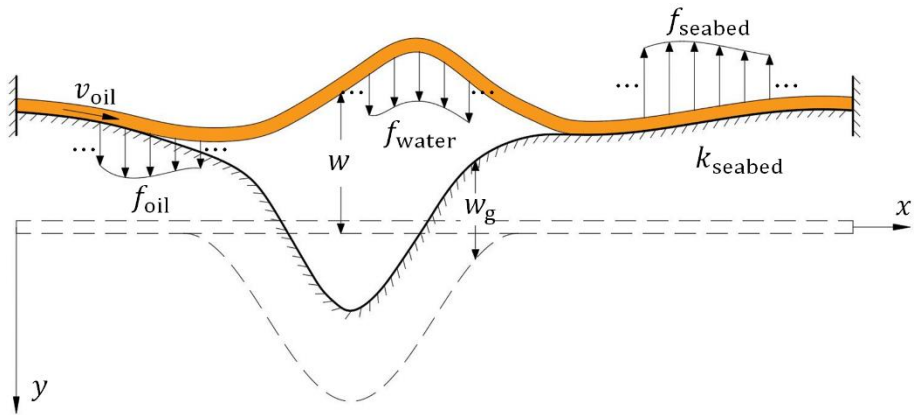
120 probability. Hence, when the failure probability is very small, e.g., of order 10^{-3} , this
121 method will suffer from inefficiency due to its demand for a large number of samples. In
122 order to reduce the computational cost of the MCS, an advanced MCS called Importance
123 Sampling (IS) was developed [21,22]. The IS requires prior knowledge of the system in
124 the failure region, so it works well when applied to a linear and low-dimensional problem,
125 whose failure region is quite simple. However, the failure region geometry of subsea
126 pipelines under an earthquake is complicated and prior knowledge of the random
127 responses is unavailable, hence the IS is not suitable for the problem considered in this
128 paper. In order to carry out reliability analysis with small failure probabilities, Au et al.
129 [23,24] developed another advanced MCS named Subset Simulation (SS). The basic idea
130 of SS is to express a small failure probability event as a product of a series of intermediate
131 events with larger conditional probabilities. Through setting these intermediate events
132 properly, the conditional probabilities can be large enough to be estimated with a small
133 number of samples. SS is a robust and efficient method and has been used for predicting
134 small failure probabilities in engineering fields, such as the time-dependent reliability of
135 underground flexible pipelines [25], the probabilistic dynamic behaviour of mistuned
136 bladed disc systems [26], radioactive waste repository performance assessment [27], the
137 stochastic dynamic stiffness of foundations for large offshore wind turbines [28] and so
138 on. A general form of SS is presented in [29] is mainly, with application to a seismic risk
139 problem involving dynamic analysis.

140 As mentioned above, reliability analysis of subsea pipelines subjected to random
141 earthquakes faces two difficulties: the solution of random responses and estimation of
142 reliability, and these are the focus of this paper. Regarding random response solutions,
143 mathematical models with reasonable simplifications and assumptions are firstly
144 estimated for pipelines, seabed and ground motions, and then a corresponding solution
145 strategy is given based on LCP. Regarding reliability estimation, SS is introduced to
146 increase the computational efficiency for the predictions of first-excursion failure
147 probabilities of pipelines. This paper therefore provides a practical computational
148 framework for the reliability analysis of subsea pipelines subjected to random
149 earthquakes. The work is structured as follows. In section 2, the mathematical formulation
150 of a subsea pipeline under a random earthquake is given. In section 3, by combining the
151 finite element method and Newmark integration method, a solution strategy is obtained
152 by deriving the unilateral contact problem as a LCP. In section 4 the fundamental concept
153 and implementation procedures of SS are briefly presented. Section 5 gives some
154 numerical examples. The feasibility of SS is verified with respect to direct MCS, and the
155 contribution of some random parameters to the failure of pipelines is addressed through
156 a sensitivity analysis. Then, influences of the unilateral contact effect, the spatial variation
157 and the free span on the reliability of pipelines are investigated. Finally, conclusions are
158 given in section 6.

159



(a) Without deformation



(b) With deformation

Fig. 1. Schematic of a subsea pipeline

2 Problem formulations

2.1 Governing equations of the pipeline

A schematic of a subsea pipeline and the seabed is shown in Fig. 1(a). There is a free span in the middle of the pipeline due to the scouring or unevenness of the seabed. The length of the pipeline is denoted by L_0 , while the location and length of the free span are denoted by L_1 and L_2 , respectively. Because of the complex formation mechanism and

173 the lack of practical measured data of the free span, the seabed profile $w_g^{(0)}$ is
 174 approximated with the following function

$$175 \quad w_g^{(0)} = \begin{cases} 0 & 0 \leq x < L_1 - L_2/2 \\ \frac{h_{\text{free}}}{2} \left[1 - \cos \frac{2\pi(x - L_1 + L_2/2)}{L_2} \right] & L_1 - L_2/2 \leq x < L_1 + L_2/2 \\ 0 & L_1 + L_2/2 \leq x \leq L_0 \end{cases} \quad (1)$$

176
 177 where h_{free} is the maximum depth of the free span.

178 The pipeline is modelled based on the Timoshenko beam theory and hydrodynamic
 179 forces of the internal oil and the surrounding seawater are considered. The seabed is
 180 simplified as a Winkler foundation. In the coordinates shown in Fig. 1(b), the governing
 181 equations for the vibration of the pipeline in the vertical plane can be written as

$$182 \quad \begin{aligned} & \rho I \frac{\partial^2 \theta}{\partial t^2} - EI \frac{\partial^2 \theta}{\partial x^2} - \kappa GA \left(\frac{\partial w}{\partial x} - \theta \right) + d_1 \rho I \frac{\partial \theta}{\partial t} \\ & \quad - d_2 \left[EI \frac{\partial^3 \theta}{\partial x^2 \partial t} + \kappa GA \left(\frac{\partial^2 w}{\partial x \partial t} - \frac{\partial \theta}{\partial t} \right) \right] = M_{\text{oil}} \\ m_{\text{pipe}} \frac{\partial^2 w}{\partial t^2} - \kappa GA \left(\frac{\partial^2 w}{\partial x^2} - \frac{\partial \theta}{\partial x} \right) + d_1 m_{\text{pipe}} \frac{\partial w}{\partial t} - d_2 \kappa GA \left(\frac{\partial^3 w}{\partial x^2 \partial t} - \frac{\partial^2 \theta}{\partial x \partial t} \right) \\ & \quad + N_0 \frac{\partial^2 w}{\partial x^2} = f_{\text{oil}} + f_{\text{water}} - f_{\text{seabed}} \end{aligned} \quad (2)$$

183
 184 where t is time, θ is the cross-section rotation, w is the vertical displacement of the
 185 pipeline, ρI is the moment of inertia, EI is the flexural rigidity, κGA is the effective
 186 shear rigidity, m_{pipe} is the mass per unit length, d_1 and d_2 are Rayleigh damping
 187 factors corresponding to the mass and stiffness, respectively, N_0 is the axial compression,
 188 M_{oil} and f_{oil} are respectively the hydrodynamic forces per unit length in the rotational

189 and vertical directions, f_{water} is the hydrodynamic force per unit length due to the
 190 surrounding seawater, and f_{seabed} is the reaction force per unit length of the seabed.

191 It is assumed that the internal oil is an incompressible and inviscid fluid with a
 192 constant flow velocity v_{oil} , and the effects of the oil are considered as external forces on
 193 the pipeline. Thus, as a fluid-conveying beam [30], M_{oil} and f_{oil} can be expressed as
 194

$$\begin{aligned}
 M_{\text{oil}} &= -\rho_{\text{oil}} I_{\text{oil}} \frac{\partial^2 \theta}{\partial x^2} \\
 f_{\text{oil}} &= -m_{\text{oil}} v_{\text{oil}}^2 \frac{\partial^2 w}{\partial x^2} - 2m_{\text{oil}} v_{\text{oil}} \frac{\partial^2 w}{\partial x \partial t} - m_{\text{oil}} \frac{\partial^2 w}{\partial t^2}
 \end{aligned} \tag{3}$$

195
 196 in which $\rho_{\text{oil}} I_{\text{oil}}$ is the moment of inertia of the oil and m_{oil} is its mass per unit length.

197 For slender cylindrical structures such as pipelines, Morison's equation [31] is
 198 widely used to evaluate the resulting hydrodynamic force of the surrounding water,
 199 defined as the summation of the inertia and drag forces. It is assumed that the surrounding
 200 water is static, while the drag force is small and hence can be neglected, so that f_{water} is
 201 determined by

$$f_{\text{water}} = -C_m \rho_{\text{water}} \pi R_{\text{out}}^2 \frac{\partial^2 w}{\partial t^2} \tag{4}$$

202
 203 where C_m is the added mass coefficient and is generally equal to 1.0, ρ_{water} is the
 204 density of the seawater and R_{out} is the outer radius of the pipe.

205
 206 The friction of the seabed is ignored. Unilateral contact in the vertical plane is
 207 considered, and thus the reaction force of the seabed f_{seabed} is

208

$$f_{\text{seabed}} = \begin{cases} 0 & \xi > 0 \\ \lambda k_{\text{seabed}} & \xi = 0 \end{cases} \quad (5)$$

209

210 where k_{seabed} is the stiffness of the seabed, and

211

$$\xi = \lambda + w_{\text{g}}^{(0)} + w_{\text{g}} - w \quad (6)$$

212

213 is the relative displacement between the pipe and the seabed, λ is the compressional

214 deformation of the seabed, $w_{\text{g}}^{(0)}$ is the initial profile of the seabed and w_{g} is the motion

215 of the seabed. Since the pipeline is constrained unilaterally by the seabed, the reaction of

216 the seabed can only be compressive, but not tensile. On the other hand, the pipe can be

217 either above or in contact with the seabed, but never under it. Hence, f_{seabed} and ξ

218 satisfy the following linear complementarity conditions,

219

$$\xi \geq 0, \quad f_{\text{seabed}} \geq 0, \quad \xi f_{\text{seabed}} = 0 \quad (7)$$

220

221 Obtaining the solution of Eq. (2) is a quite challenging task because of two

222 difficulties. Firstly, the earthquake is a random process and the spatial variation is

223 considered, so the motion of the seabed is actually a random field. Secondly, contact

224 regions of the pipeline and seabed are not known a priori and will change with the pipeline

225 motion. The contact nonlinearity further increases the difficulty of solution.

226 **2.2 Random earthquake with spatial variation**

227 The acceleration of the ground motion due to the earthquake is assumed to be a

228 nonstationary random process which can be expressed as

229

$$\ddot{w}_g = g(t)\ddot{d}(t) \quad (8)$$

230

231 where $\ddot{d}(t)$ is a stationary Gaussian random process with zero mean value and $g(t)$ is

232 a slowly varying deterministic envelope function which is given as

233

$$g(t) = 2.5974(e^{-0.2t} - e^{-0.6t}) \quad (9)$$

234

235 Assuming that $\ddot{d}(t)$ is homogeneous in the spatial domain, then the cross power

236 spectral density (PSD) of the acceleration at two arbitrary points can be expressed as

237

$$S(\Delta x, \omega) = \gamma(\Delta x, \omega)S_0(\omega) \quad (10)$$

238

239 where ω is the circular frequency, $\Delta x = |x_i - x_j|$ is the distance between the two

240 points x_i and x_j on the ground, $S_0(\omega)$ is the auto-PSD of the acceleration of the

241 ground motion and $\gamma(\Delta x, \omega)$ is the coherency function which can be written as

242

$$\gamma(\Delta x, \omega) = \gamma^{(w)}(\Delta x, \omega)\gamma^{(c)}(\Delta x, \omega) \quad (11)$$

243

244 in which

245

$$\gamma^{(w)}(\Delta x, \omega) = \exp\left(-\frac{i\omega\Delta x}{v_{app}}\right) \quad (12)$$

246

247 indicates the complex-valued wave passage effect, $i = \sqrt{-1}$, v_{app} is the apparent

248 velocity of the earthquake waves, and

249

$$\gamma^{(c)}(\Delta x, \omega) = \exp\left(-\alpha \frac{\omega \Delta x}{2\pi v_{\text{app}}}\right) \quad (13)$$

250

251 characterizes the real-valued incoherence effect. The L-Y model [32] is used in this paper

252 and $\alpha = 0.125$. The modified Kanai-Tajimi PSD of the acceleration is used and S_0 is

253 given by [33]

254

$$S_0(\omega) = \frac{1 + 4\xi_g^2(\omega/\omega_g)^2}{\left[1 - (\omega/\omega_g)^2\right]^2 + 4\xi_g^2(\omega/\omega_g)^2} \times \frac{(\omega/\omega_f)^4}{\left[1 - (\omega/\omega_f)^2\right]^2 + 4\xi_f^2(\omega/\omega_f)^2} S_g \quad (14)$$

255

256 where ω_g and ξ_g are the resonant frequency and damping ratio of the first filter, and

257 ω_f and ξ_f are those of the second filter. S_g is the amplitude of the white-noise bedrock

258 acceleration which depends on the soil condition.

259 Since the SS used in this paper is based on the MCS method, the time history samples

260 of the ground motion should be generated from the PSD of the acceleration as shown in

261 Eq. (10). Here the Auto-Regressive Moving-Average (ARMA) method is used to generate

262 the time history samples of the ground acceleration. For brevity in this paper, details of

263 the ARMA are not presented and interested readers are referred to [34]. In addition, since

264 it is required to estimate the force acting on the pipeline, and to detect the contact between

265 the pipeline and the seabed in each time step, the time histories of the velocity and

266 displacement of the seabed also need to be evaluated. A simple and direct approach to

267 obtaining the velocity and displacement is to make use of the inherent integral relations
 268 between the displacement, velocity and acceleration by assuming zero initial conditions.
 269 However, due to the accumulation of random noise in accelerations, direct integration of
 270 the acceleration data often causes unrealistic drifts, namely baseline offsets in the velocity
 271 and displacement. In order to eliminate the baseline offsets, a commonly used correction
 272 scheme suggested by Berg and Housner [35] is used, in which the zero-acceleration
 273 baseline is assumed to be of polynomial form, the constants of which are determined by
 274 minimizing the mean square computed velocity.

275

276 **3 Linear complementarity method for the dynamic contact of** 277 **pipeline and seabed**

278 Because of the contact nonlinearity, it is impossible to obtain an analytical solution
 279 of Eq. (2). Numerical solution seems to be the only choice, and thus a suitable
 280 discretization is needed in the spatial and time domains. The pipeline is discretized into
 281 Timoshenko beam elements with two nodes, considering the effects of both the oil
 282 conveyed through the pipeline and the surrounding seawater, while the seabed is modelled
 283 as spring elements. Considering the spatial variation of the ground motion, the governing
 284 equation of the pipeline can be represented in the following discrete form,

285

$$\begin{bmatrix} \mathbf{M}_s & \mathbf{M}_{sb} \\ \mathbf{M}_{sb}^T & \mathbf{M}_b \end{bmatrix} \begin{Bmatrix} \ddot{\mathbf{X}}_s \\ \ddot{\mathbf{X}}_b \end{Bmatrix} + \begin{bmatrix} \mathbf{C}_s & \mathbf{C}_{sb} \\ \mathbf{C}_{sb}^T & \mathbf{C}_b \end{bmatrix} \begin{Bmatrix} \dot{\mathbf{X}}_s \\ \dot{\mathbf{X}}_b \end{Bmatrix} + \begin{bmatrix} \mathbf{K}_s & \mathbf{K}_{sb} \\ \mathbf{K}_{sb}^T & \mathbf{K}_b \end{bmatrix} \begin{Bmatrix} \mathbf{X}_s \\ \mathbf{X}_b \end{Bmatrix} = \begin{Bmatrix} \mathbf{R}_s \\ \mathbf{R}_b \end{Bmatrix} \quad (15)$$

286

287 in which the subscripts “b” and “s” indicate the support and non-support degrees of
 288 freedom (DOF), respectively, so that \mathbf{X}_b are the enforced displacements of the supports
 289 on both sides, \mathbf{X}_s are all nodal displacements except those at the supports, \mathbf{R}_b are the
 290 enforced forces at the supports and \mathbf{R}_s are the reaction forces of the seabed. \mathbf{M} , \mathbf{C} and
 291 \mathbf{K} are the mass, damping and stiffness matrices, respectively. Expanding the first row of
 292 Eq. (15) gives
 293

$$\mathbf{M}_s \ddot{\mathbf{X}}_s + \mathbf{C}_s \dot{\mathbf{X}}_s + \mathbf{K}_s \mathbf{X}_s = \mathbf{R}_s + \mathbf{P} \quad (16)$$

294 where $\mathbf{P} = -\mathbf{M}_{sb} \ddot{\mathbf{X}}_b - \mathbf{C}_{sb} \dot{\mathbf{X}}_b - \mathbf{K}_{sb} \mathbf{X}_b$ is the effective earthquake force acting on the
 295 non-support DOF.
 296

297 Each node of the beam element used in this paper has two DOF, namely translation
 298 and rotation in the vertical plane. However, it is assumed that the reaction force of the
 299 seabed acts only on the translation DOF. For the convenience of the following derivation
 300 procedures, rearranging the DOF in Eq. (16) gives
 301

$$\begin{aligned} & \begin{bmatrix} \mathbf{M}_w & \mathbf{M}_{wq} \\ \mathbf{M}_{qw} & \mathbf{M}_q \end{bmatrix} \begin{Bmatrix} \ddot{\mathbf{w}} \\ \ddot{\mathbf{q}} \end{Bmatrix} + \begin{bmatrix} \mathbf{C}_w & \mathbf{C}_{wq} \\ \mathbf{C}_{qw} & \mathbf{C}_q \end{bmatrix} \begin{Bmatrix} \dot{\mathbf{w}} \\ \dot{\mathbf{q}} \end{Bmatrix} + \begin{bmatrix} \mathbf{K}_w & \mathbf{K}_{wq} \\ \mathbf{K}_{qw} & \mathbf{K}_q \end{bmatrix} \begin{Bmatrix} \mathbf{w} \\ \mathbf{q} \end{Bmatrix} \\ & = \begin{Bmatrix} \mathbf{r}_w \\ \mathbf{0} \end{Bmatrix} + \begin{Bmatrix} \mathbf{P}_w \\ \mathbf{P}_q \end{Bmatrix} \end{aligned} \quad (17)$$

302 where \mathbf{w} and \mathbf{q} are the translation and rotation DOF, respectively; \mathbf{P}_w and \mathbf{P}_q are
 303 the effective forces acting on the translation and rotation DOF, respectively, and \mathbf{r}_w is
 304 the reaction force of the seabed.
 305

306 Based on the Newmark integration method, Eq. (17) is discretized in the time domain.

307 With appropriate gathering of terms, the governing equation at time t_{k+1} can be written

308 as

309

$$\begin{bmatrix} \widehat{\mathbf{K}}_w & \widehat{\mathbf{K}}_{wq} \\ \widehat{\mathbf{K}}_{qw} & \widehat{\mathbf{K}}_q \end{bmatrix} \begin{Bmatrix} \mathbf{w} \\ \mathbf{q} \end{Bmatrix}_{k+1} = \begin{Bmatrix} \mathbf{r}_w \\ \mathbf{0} \end{Bmatrix}_{k+1} + \begin{Bmatrix} \widehat{\mathbf{P}}_w \\ \widehat{\mathbf{P}}_q \end{Bmatrix}_{k+1} \quad (18)$$

310

311 where

312

$$\begin{bmatrix} \widehat{\mathbf{K}}_w & \widehat{\mathbf{K}}_{wq} \\ \widehat{\mathbf{K}}_{qw} & \widehat{\mathbf{K}}_q \end{bmatrix} = \begin{bmatrix} \mathbf{K}_w & \mathbf{K}_{wq} \\ \mathbf{K}_{qw} & \mathbf{K}_q \end{bmatrix} + a_0 \begin{bmatrix} \mathbf{M}_w & \mathbf{M}_{wq} \\ \mathbf{M}_{qw} & \mathbf{M}_q \end{bmatrix} + a_1 \begin{bmatrix} \mathbf{C}_w & \mathbf{C}_{wq} \\ \mathbf{C}_{qw} & \mathbf{C}_q \end{bmatrix} \quad (19)$$

313

$$\begin{Bmatrix} \widehat{\mathbf{P}}_w \\ \widehat{\mathbf{P}}_q \end{Bmatrix}_{k+1} = \begin{Bmatrix} \mathbf{P}_w \\ \mathbf{P}_q \end{Bmatrix}_{k+1} + \begin{bmatrix} \mathbf{M}_w & \mathbf{M}_{wq} \\ \mathbf{M}_{qw} & \mathbf{M}_q \end{bmatrix} \left(a_0 \begin{Bmatrix} \mathbf{w} \\ \mathbf{q} \end{Bmatrix}_k + a_2 \begin{Bmatrix} \dot{\mathbf{w}} \\ \dot{\mathbf{q}} \end{Bmatrix}_k + a_3 \begin{Bmatrix} \ddot{\mathbf{w}} \\ \ddot{\mathbf{q}} \end{Bmatrix}_k \right) \\ + \begin{bmatrix} \mathbf{C}_w & \mathbf{C}_{wq} \\ \mathbf{C}_{qw} & \mathbf{C}_q \end{bmatrix} \left(a_1 \begin{Bmatrix} \mathbf{w} \\ \mathbf{q} \end{Bmatrix}_k + a_4 \begin{Bmatrix} \dot{\mathbf{w}} \\ \dot{\mathbf{q}} \end{Bmatrix}_k + a_5 \begin{Bmatrix} \ddot{\mathbf{w}} \\ \ddot{\mathbf{q}} \end{Bmatrix}_k \right) \quad (20)$$

314

$$a_0 = \frac{1}{\alpha(\Delta t)^2} \quad a_1 = \frac{\delta}{\alpha\Delta t} \quad a_2 = \frac{1}{\alpha\Delta t} \quad a_3 = \frac{1}{2\alpha} - 1 \\ a_4 = \frac{\delta}{\alpha} - 1 \quad a_5 = \frac{\Delta t}{2} \left(\frac{\delta}{\alpha} - 2 \right) \quad (21)$$

315

316 in which Δt is the time step, δ and α are parameters of the Newmark integration

317 method, which satisfy $\delta \geq 0.5$ and $\alpha \geq 0.25(0.5 + \delta)^2$ to ensure the unconditional

318 stability of the integration scheme. The acceleration and the velocity at time t_{k+1} are

319

$$\begin{Bmatrix} \ddot{\mathbf{w}} \\ \ddot{\mathbf{q}} \end{Bmatrix}_{k+1} = a_0 \left(\begin{Bmatrix} \mathbf{w} \\ \mathbf{q} \end{Bmatrix}_{k+1} - \begin{Bmatrix} \mathbf{w} \\ \mathbf{q} \end{Bmatrix}_k \right) - a_2 \begin{Bmatrix} \dot{\mathbf{w}} \\ \dot{\mathbf{q}} \end{Bmatrix}_k - a_3 \begin{Bmatrix} \ddot{\mathbf{w}} \\ \ddot{\mathbf{q}} \end{Bmatrix}_k \\ \begin{Bmatrix} \dot{\mathbf{w}} \\ \dot{\mathbf{q}} \end{Bmatrix}_{k+1} = \begin{Bmatrix} \dot{\mathbf{w}} \\ \dot{\mathbf{q}} \end{Bmatrix}_k + a_6 \begin{Bmatrix} \ddot{\mathbf{w}} \\ \ddot{\mathbf{q}} \end{Bmatrix}_k + a_7 \begin{Bmatrix} \ddot{\mathbf{w}} \\ \ddot{\mathbf{q}} \end{Bmatrix}_{k+1} \quad (22)$$

320

321 in which $a_6 = \Delta t(1 - \delta)$ and $a_7 = \delta\Delta t$.

322 Expanding Eq. (18) and eliminating terms related to \mathbf{q} gives

323

$$\bar{\mathbf{K}}_w \mathbf{w}_{k+1} = \mathbf{r}_{w,k+1} + \bar{\mathbf{P}}_{w,k+1} \quad (23)$$

324

325 where $\bar{\mathbf{K}}_w = \hat{\mathbf{K}}_w - \hat{\mathbf{K}}_{wq} \hat{\mathbf{K}}_q^{-1} \hat{\mathbf{K}}_{qw}$ and $\bar{\mathbf{P}}_{w,k+1} = \hat{\mathbf{P}}_{w,k+1} - \hat{\mathbf{K}}_{wq} \hat{\mathbf{K}}_q^{-1} \hat{\mathbf{P}}_{q,k+1}$.

326 According to Eq. (6), the relative vertical distance between the seabed and pipeline

327 at time t_{k+1} is

328

$$\xi_{k+1} = \lambda_{k+1} + \mathbf{w}_g^{(0)} + \mathbf{w}_{g,k+1} - \mathbf{w}_{k+1} \quad (24)$$

329

330 where

331

$$\lambda_{k+1} = \mathbf{K}_g^{-1} \mathbf{r}_{w,k+1} \quad (25)$$

332

333 is the compressional deformation of the seabed at time t_{k+1} , \mathbf{K}_g is the stiffness matrix

334 of the seabed and $\mathbf{w}_g^{(0)}$ is the initial profile of the seabed.

335 Combining Eqs. (23) to (25) gives

336

$$\tilde{\mathbf{K}} \xi_{k+1} = \mathbf{r}_{w,k+1} + \tilde{\mathbf{P}}_{w,k+1} \quad (26)$$

337

338 in which $\tilde{\mathbf{K}} = (\bar{\mathbf{K}}_w \mathbf{K}_g^{-1} - \mathbf{I})^{-1} \bar{\mathbf{K}}_w$, $\tilde{\mathbf{P}}_{w,k+1} = (\bar{\mathbf{K}}_w \mathbf{K}_g^{-1} - \mathbf{I})^{-1} [\bar{\mathbf{K}}_w (\mathbf{w}_g^{(0)} + \mathbf{w}_{g,k+1}) -$

339 $\bar{\mathbf{P}}_{w,k+1}]$ and \mathbf{I} is an identity matrix.

340 Eq. (7) can be expressed in the following discretized form

341

$$\boldsymbol{\xi}_{k+1} \geq \mathbf{0}, \quad \mathbf{r}_{w,k+1} \geq \mathbf{0}, \quad \boldsymbol{\xi}_{k+1}^T \mathbf{r}_{w,k+1} = 0 \quad (27)$$

342

343 Eqs. (26) and (27) together form a mathematical structure known as a LCP, which is

344 equivalent to the following quadratic programming problem

345

$$\begin{aligned} \min f(\boldsymbol{\xi}_{k+1}) &= \frac{1}{2} \boldsymbol{\xi}_{k+1}^T \tilde{\mathbf{K}} \boldsymbol{\xi}_{k+1} - \tilde{\mathbf{P}}_{w,k+1}^T \boldsymbol{\xi}_{k+1} \\ \text{s. t. } &\boldsymbol{\xi}_{k+1} \geq \mathbf{0} \end{aligned} \quad (28)$$

346

347 Because of the symmetry and positive definiteness of $\tilde{\mathbf{K}}$, Eq. (28) is a convex

348 optimization problem and the common solution to it is guaranteed to exist and be unique

349 [12]. There are many well-developed methods to solve the LCP and most of them have

350 been included in some commercial software. For simplicity, the solution procedures of

351 the LCP are not given in this paper.

352 By solving the LCP problem of Eq. (28), $\boldsymbol{\xi}_{k+1}$ can be determined. Then, by

353 substituting $\boldsymbol{\xi}_{k+1}$ into Eq. (26), the reaction force of the seabed $\mathbf{r}_{w,k+1}$ is obtained. The

354 displacement of the pipeline \mathbf{w}_{k+1} is further determined by substituting $\mathbf{r}_{w,k+1}$ into Eq.

355 (23). It is worthwhile to point out that an iterative procedure is needed in most solution

356 methods for the LCP, and thus the solution at the current time step can be used as the

357 initial trial solution for the next time step in order to accelerate convergence.

358

359 **4 Subset simulation for reliability estimation**

360 The first-excursion probabilities of a subsea pipeline subjected to a spatially varying

361 ground motion are considered in this paper. The failure event of the pipelines can be
 362 represented as the exceedance of an arbitrary response $\mathbf{s}(t, \boldsymbol{\theta})$, which can be the
 363 displacement, internal force, stress or any other response, above the threshold value b
 364 within a specified time interval, i.e.,

$$F = \left\{ \max_{l=1, \dots, n_r} \left(\max_{t \in [0, T]} |\mathbf{s}(t, \boldsymbol{\theta})| \right) > b \right\} \quad (29)$$

366 where n_r denotes the dimension of the response $\mathbf{s}(t, \boldsymbol{\theta})$, T is the duration of the
 367 earthquake, $\boldsymbol{\theta}$ is a random variable vector which characterizes the randomness in the
 368 system, and whose probability density function (PDF) is $q(\boldsymbol{\theta})$. It is noted that bending
 369 stresses are used to identify the failure of pipelines in this paper. The probability of the
 370 occurrence of the failure event F , namely, the failure probability, can be expressed in
 371 terms of the following probability integral

$$P(F) = \int_{\boldsymbol{\theta} \in \boldsymbol{\Omega}} I_F(\boldsymbol{\theta}) q(\boldsymbol{\theta}) d\boldsymbol{\theta} \quad (30)$$

374 where I_F is the indicator function, which is equal to 1 when the pipeline has failed and
 375 0 otherwise. $\boldsymbol{\Omega}$ denotes the value space of $\boldsymbol{\theta}$.

377 Generally, the integral in Eq. (30) cannot be calculated efficiently by means of direct
 378 numerical integration due to the high dimension of $\boldsymbol{\theta}$ and the complicated geometry of
 379 the failure region. MCS is commonly used in problems with high dimension and a
 380 complicated failure region, by virtue of its computational robustness. However, the main

381 drawback of MCS is that it is not suitable for evaluating small failure probabilities due to
 382 its demand for a large number of samples. In order to reduce the computational cost of
 383 MCS, SS [23, 24] is used, of which the main procedures are as follows.

384 By introducing a sequence of ascending threshold values $0 < b_1 < b_2 < \dots <$
 385 $b_n = b$, one can obtain the corresponding intermediate failure events $F_1 \supset F_2 \supset \dots \supset$
 386 $F_n = F$. By the definition of conditional probability, the failure probability of the pipeline
 387 can be expressed as a product of conditional probabilities,

$$P(F) = P(F_1) \prod_{i=1}^{n-1} P(F_{i+1}|F_i) = \prod_{i=1}^n P_i \quad (31)$$

389 where P_1 denotes $P(F_1)$ and $P_i (i = 2, 3, \dots, n)$ denotes $P(F_i|F_{i-1})$. Eq. (32)
 390 expresses a small failure probability as a product of relatively large conditional
 391 probabilities. For example, assume $P_i \sim 0.1, i = 1, 2, \dots, 4$, then the failure probability
 392 $P(F) \sim 10^{-4}$ which is too small for efficient estimation by MCS. However, the
 393 conditional probabilities $P_i (i = 1, 2, \dots, 4)$, are of order 0.1, and so can be evaluated
 394 efficiently by simulation.

396 The probability P_1 can be evaluated readily by the application of direct MCS
 397 simulation as

$$P_1 = \frac{1}{N_1} \sum_{h=1}^{N_1} I_{F_1}(\theta_h^{(1)}) \quad (32)$$

399

400 in which $\boldsymbol{\theta}_h^{(1)}$ ($h = 1, 2, \dots, N_1$) are independently distributed samples simulated from
 401 the PDF $q(\boldsymbol{\theta})$, and N_1 is the number of samples $\boldsymbol{\theta}_h^{(1)}$.

402 To estimate the conditional probabilities P_i ($i = 2, 3, \dots, n$) samples should be
 403 generated according to the conditional PDF $q(\boldsymbol{\theta}|F_{i-1}) = q(\boldsymbol{\theta})I_{F_i}(\boldsymbol{\theta})/P(F_{i-1})$. However,
 404 efficient sampling from a conditional PDF is usually not a trivial task. Fortunately, this
 405 can be achieved by the Markov chain Monte Carlo (MCMC) simulation based on the
 406 Metropolis-Hastings (M-H) algorithm which provides a powerful method for generating
 407 samples that satisfy the prescribed conditional probability. Readers are referred to [23]
 408 for more details regarding the MCMC and the modified M-H algorithm.

409 After generating the conditional samples, the conditional failure probability P_i can
 410 be determined as

411

$$P_i = \frac{1}{N_i} \sum_{h=1}^{N_i} I_{F_i}(\boldsymbol{\theta}_h^{(i)}) \quad (33)$$

412

413 where $\boldsymbol{\theta}_h^{(i)}$ ($h = 1, 2, \dots, N_i$) are independent distributed conditional samples according
 414 to the conditional density probability $q(\boldsymbol{\theta}|F_{i-1})$. Through choosing the intermediate
 415 threshold values b_i adaptively, the conditional probabilities P_i ($i = 1, 2, \dots, n - 1$) can
 416 be ensured to be equal to a certain value p_0 ($p_0 = 0.1$ is used here). Substituting Eqs.
 417 (32) and (33) into Eq. (31), the failure probability can be expressed as

418

$$P_F = p_0^{n-1} \frac{1}{N_n} \sum_{h=1}^{N_n} I_{F_n}(\boldsymbol{\theta}_h^{(n)}) \quad (34)$$

419

420 The main procedures of SS can be summarized as follows.

421 1. Generate N samples $\boldsymbol{\theta}_h^{(0)} (h = 1, 2, \dots, N)$ by direct MCS from the original PDF

422 $q(\boldsymbol{\theta})$. The superscript “0” denotes these samples correspond to conditional level 0.

423 2. Set $i = 0$.

424 3. Calculate the corresponding response variable $\tilde{\mathbf{s}}(\boldsymbol{\theta}_h^{(i)}) = \max(|\mathbf{s}(t, \boldsymbol{\theta}_h^{(i)})|)$

425 4. Choose the intermediate threshold value b_{i+1} as the $(1 - p_0)N$ th value in the

426 ascending order of $\tilde{\mathbf{s}}(\boldsymbol{\theta}_h^{(i)})$ (calculated at step 3). Hence the sample estimate of P_{i+1} is

427 always equal to p_0 . Note that it has been assumed that p_0N is an integer value.

428 5. If $b_{i+1} > b_n$, proceed to step 10 below.

429 6. Otherwise, if $b_{i+1} < b$, with the choice of b_{i+1} performed at step 4, identify the

430 p_0N samples $\boldsymbol{\theta}_H^{(i)} (H = 1, 2, \dots, p_0N)$ among $\boldsymbol{\theta}_h^{(i)} (h = 1, 2, \dots, N)$ whose response

431 $\tilde{\mathbf{s}}(\boldsymbol{\theta}_H^{(i)})$ lies in the region $F_{i+1} = \{\tilde{\mathbf{s}}(\boldsymbol{\theta}_H^{(i)}) > b_{i+1}\}$. These samples are at conditional

432 level $i + 1$ and distributed as the conditional probability $q(\cdot | F_{i+1})$.

433 7. The samples $\boldsymbol{\theta}_H^{(i)} (H = 1, 2, \dots, p_0N)$ (identified at step 6) provide seeds for

434 applying the MCMC simulation to generate $(1 - p_0)N$ additional conditional samples

435 distributed as the conditional probability $q(\cdot | F_{i+1})$, so that it obtains a total of N

436 conditional samples $\boldsymbol{\theta}_h^{(i+1)} (h = 1, 2, \dots, N) \in F_{i+1}$ at conditional level $i + 1$.

437 8. Set $i \leftarrow i + 1$.

438 9. Return to step 3 above.

439 10. Stop the algorithm.

440 It is noted that the total number of samples employed is $N_T = N + (n - 1)(1 -$
 441 $p_0)N$.

442 The sensitivity of the reliability with respect to variations in system parameters
 443 reflects the contributions of these parameters to the failure of structures, and hence it is
 444 useful to perform a reliability sensitivity analysis. The reliability sensitivity is defined as
 445 the partial derivative of the failure probability with respect to distributional parameters of
 446 the system parameter. In the framework of SS, the reliability sensitivity can be expressed
 447 as [36]

$$\frac{\partial P_F}{\partial \eta} \Big|_{\bar{\eta}} = p_0^{n-1} \frac{1}{N_n} \sum_{h=1}^{N_n} I_{F_n}(\boldsymbol{\theta}_h^{(n)}) \frac{\partial q(\boldsymbol{\theta}_h^{(n)})}{q(\boldsymbol{\theta}_h^{(n)})} \quad (35)$$

449 where η denotes the distribution parameters, for example, the mean value or the standard
 450 deviation, of the PDF of the uncertain system parameters $\boldsymbol{\theta}$. $\bar{\eta}$ is the value of the
 451 distribution parameter where the sensitivity is evaluated. For a better comparison of the
 452 contribution of different system parameters, the reliability sensitivity can be normalized
 453 as follows,

$$e_\eta = \frac{\partial P_F}{\partial \eta} \frac{\bar{\eta}}{P_F} \quad (36)$$

456

457 **5 Numerical examples**

458 In the following numerical examples, information about the system parameters is

459 given first. Then, SS is applied for estimating the failure probability of a subsea pipeline
460 subjected to a random earthquake with spatial variation, and a comparison is made with
461 the direct MCS (DMCS) to verify the SS. Then a sensitivity and failure analysis is
462 performed to identify the influential parameters on the pipeline failure. Finally, the
463 reliabilities of subsea pipelines in three typical cases are investigated.

464 **5.1 Description of system parameters**

465 The subsea pipeline in Fig. 1 is adopted as an example structure. Unless otherwise
466 specified, the physical and geometric parameters of the pipeline are as follows: material
467 grade X60 with specified minimum yield strength (SMYS) $\sigma_y = 414 \times 10^6 \text{Pa}$, Young's
468 modulus $E = 207 \times 10^9 \text{Pa}$, mass density $\rho_{\text{pipe}} = 7850 \text{kg/m}^3$, Poisson's ratio $\nu =$
469 0.3 , Rayleigh damping factors corresponding to the mass $d_1 = 0.01$ and the stiffness
470 $d_2 = 0.05$, total length of pipeline $L_0 = 100 \text{m}$, shear correction factor $\kappa =$
471 $2(1 + \nu)/(4 + 3\nu)$, outer radius $R_{\text{out}} = 0.6 \text{m}$, wall thickness $h = 0.02 \text{m}$. The mass
472 densities of the oil in the pipeline and surrounding water are $\rho_{\text{oil}} = 800 \text{kg/m}^3$ and
473 $\rho_{\text{water}} = 1025 \text{kg/m}^3$, respectively, and the velocity of the oil is 3m/s . According to the
474 design standard [4], the effective axial compression N_0 should not exceed $0.5N_{\text{cr}}$,
475 where N_{cr} is the critical buckling load, and hence $N_0 = 0.3N_{\text{cr}}$ is used in this paper.
476 The pipeline is discretized into 100 elements and both ends are simply supported. The
477 failure criterion for the subsea pipeline is defined as when the bending stress exceeds 80%
478 of SMYS [37].

479 The location and length of the free span, L_1 and L_2 , are assumed to be Gaussian
480 distributed variables with mean values 50m and 30m, respectively, and coefficient of
481 variation (COV) 0.3. As physical parameters these must be strictly positive, and in order
482 to guarantee that one free span always exists, L_1 and L_2 are required to satisfy the
483 following constraints,

$$\begin{cases} L_0 \geq L_2 \geq 0 \\ L_1 - L_2/2 \geq 0 \\ L_0 - L_1 - L_2/2 \geq 0 \end{cases} \quad (37)$$

484
485
486 Strictly speaking, these constraints rule out the use of Gaussian models for the random
487 variables L_1 and L_2 . Hence, an acceptance-rejection method is used to generate samples
488 of L_1 and L_2 from Gaussian distributions with constraints as expressed in Eq. (37).

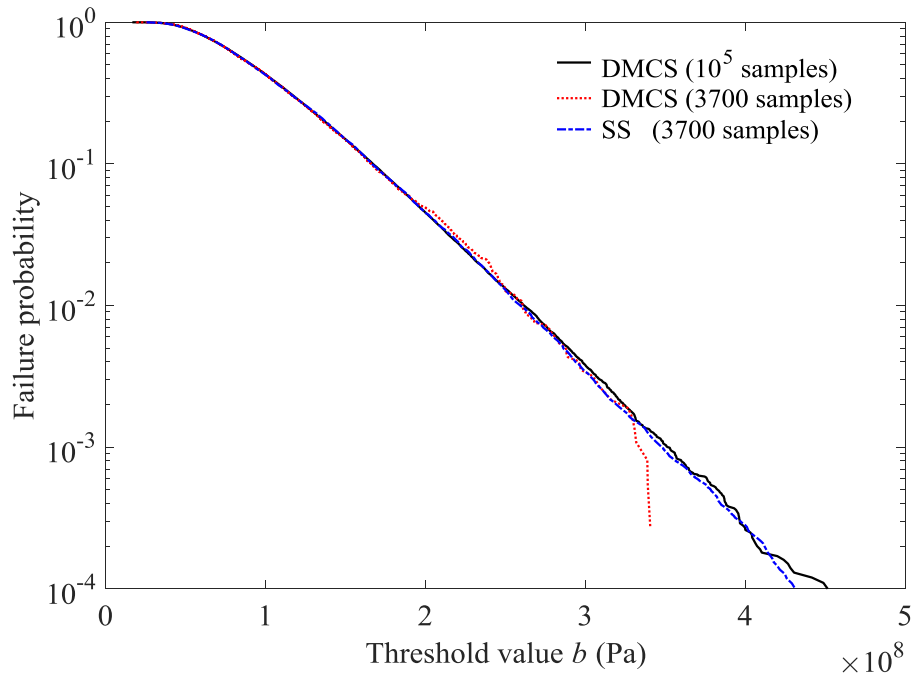
489 The maximum depth of the free span $h_{\text{free}} = 0.3\text{m}$ and the stiffness of the seabed
490 $k_{\text{seabed}} = 2.293 \times 10^6 \text{ N/m}^2$ are used here. Parameters of the ground motion PSD and
491 the spatial variation are respectively $S_g = 0.018 \text{ m}^2/\text{s}^3$, $\omega_g = 15 \text{ rad/s}$, $\omega_f = 0.1\omega_g$,
492 $v_{\text{app}} = 1000 \text{ m/s}$, $\xi_g = \xi_f = 0.6$ [38]. The duration of the earthquake is $T = 10.92\text{s}$,
493 and the time step for the numerical integration is $\Delta t = 0.01\text{s}$. Hence the number of time
494 steps is $N_t = 1093$. In order to generate the ground motion time histories from the above
495 ground PSD, the following procedures are implemented. A $N_{\text{node}} \times N_t$ discrete-time
496 white noise matrix \mathbf{W} is first generated, where the elements of \mathbf{W} have a mean value
497 of 0 and standard deviation of $\sqrt{2\pi/\Delta t}$, N_{node} is the number of nodes of the discrete
498 pipeline. Then the ARMA method is used to modulate \mathbf{W} to generate the required

499 ground motion samples.

500 During the SS procedures, the choice of the proposal PDF and the grouping of
501 uncertain parameters affect the distribution and the acceptance rate of the samples and
502 consequently the efficiency of the SS. It is suggested in [29] that deciding what type of
503 proposal PDF to use for a group depends on the contribution of the uncertain parameters
504 to the failure and on the information available for constructing the proposal PDF. In this
505 paper, there are two types of uncertain parameters. The first type is the discrete-time white
506 noise matrix \mathbf{W} , whose parameters play a similar role in affecting failure. These
507 parameters affect failure significantly as a whole, but not individually. Hence, each of
508 these parameters is grouped individually and their proposal PDFs can be chosen to be
509 uniform with width 2. The second type is the structural parameters L_1 and L_2 , whose
510 contribution to the failure cannot be known a priori. Hence, L_1 and L_2 are collected
511 into one group and the proposal PDF is chosen to be Gaussian with mean and covariance
512 estimated from the current seed samples.

513 **5.2 Validation of the subset simulation**

514 SS and DMCS are used to estimate the failure probability of the subsea pipeline
515 under the earthquake and the results are shown in Fig. 2. SS is applied with a conditional
516 failure probability $p_0 = 0.1$ and the number of samples at each level is $N = 1000$. Four
517 levels of conditional simulations are used in one simulation run, so the total number of
518 samples is $N_T = 3700$. For comparison, the failure probabilities from the DMCS with



519

520

Fig. 2. Comparison of failure probability from SS and DMCS

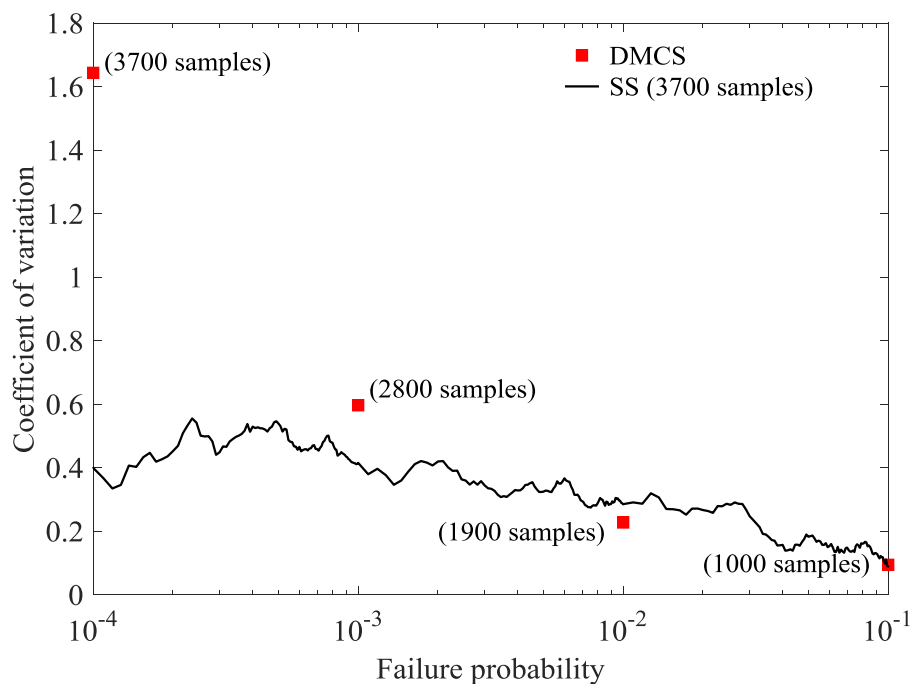
521

522 10^5 and 3700 samples are also given in Fig. 2. It is seen that the results of these three
 523 simulation cases agree very well in the region with relative large failure probability
 524 (above 10^{-2}). However, in the region with small failure probability (below 10^{-3}),
 525 results of SS and DMCS with 10^5 samples still agree quite well, while those of the
 526 DMCS with 3700 samples show a significant discrepancy.

527

528 To investigate the variability of the SS results, the COV of the failure probability
 529 from 10 independent SS runs is shown in Fig. 3. Since each conditional level contains
 530 1000 samples, the total numbers of samples, N_T , used for obtaining estimates of failure
 531 probability level at 10^{-1} , 10^{-2} , 10^{-3} and 10^{-4} are 1000, 1900, 2800 and 3700,
 respectively. For comparison, the COV of the results of the DMCS are given at particular

532 failure probability level by using the same total numbers of samples. It should be noted
533 that DMCS is unable to estimate the failure probability accurately with a relatively small
534 number of samples, e.g., 3700, so the COV of DMCS is obtained from an simple
535 approximate formula [23], i.e., $COV = \sqrt{(1 - P(F))/(P(F)N)}$, rather than from many
536 independent DMCS runs. It can be seen from Fig. 3 that the COV of SS increases
537 gradually with decreasing failure probability, while the COV of DMCS increases much
538 more rapidly. The COV of SS and DMCS are quite close in the region with relatively
539 large failure probability ($10^{-2} \sim 10^{-1}$). However, when the failure probability is below
540 10^{-3} , it can be observed that the COV of DMCS is much larger than that of SS.
541



542
543 **Fig. 3.** Comparison of the COV of the failure probabilities from SS and DMCS

544

545 The results in Fig. 2 and 3 show that, compared to DMCS, SS can estimate the failure
546 probability with much fewer samples, and its results have a smaller COV, especially in
547 the low failure probability region. Hence, SS is proved to be a highly accurate and robust
548 method to estimate the small failure probability of subsea pipelines under a random
549 earthquake.

550 **5.3 Sensitivity and failure analysis**

551 To identify the contribution of the uncertain structural parameters to the failure of
552 the subsea pipeline, a sensitivity analysis of the failure probability with respect to the
553 mean values and variations of L_1 and L_2 is performed using SS, and the results are
554 compared to those of DMCS, as shown in Table 1. It can be observed that the results of
555 SS and DMCS agree quite well from the perspective of the sensitivity which is in fact a
556 higher order quantity. It is also observed that the sensitivity with respect to L_2 is larger
557 than that with respect to L_1 , implying that the length of the free span L_2 is more
558 influential on the failure of subsea pipelines than its location L_1 .

559 The Markov chain samples generated during SS can be used not only for estimating
560 the conditional probabilities, but also for the failure probability [29]. From Bayes'
561 theorem,

562

$$P(F|\theta_l) = \frac{q(\theta_l|F)}{q(\theta_l)}P(F), \quad l = 1, 2 \dots N_\theta \quad (39)$$

563

564

565

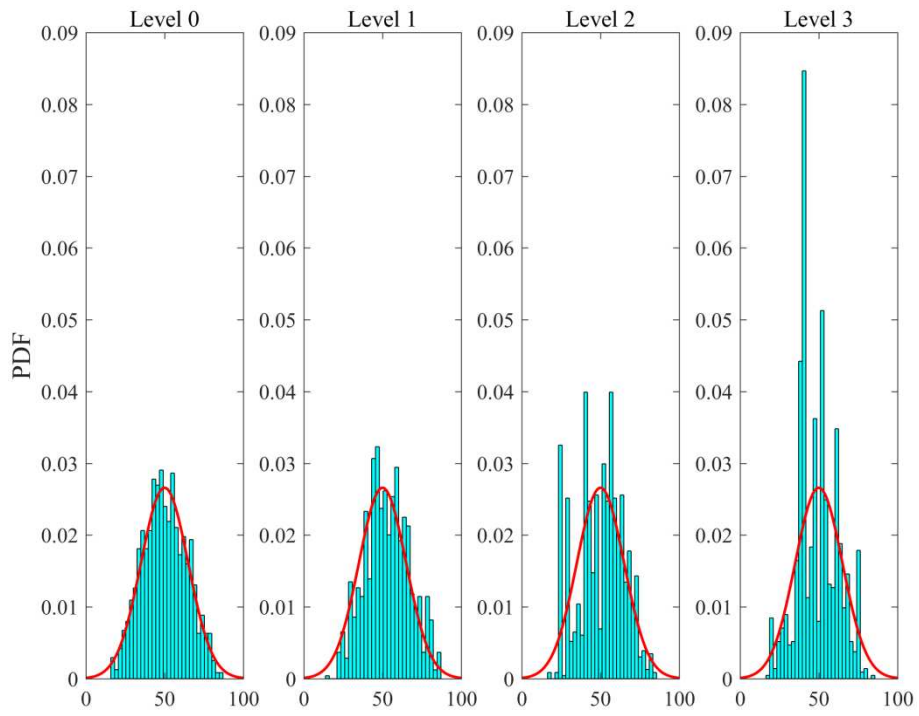
Table 1 Normalized sensitivities of the failure probability

	SS	DMCS
$e_{\mu_{L_1}}$	0.147	0.125
$e_{\mu_{L_2}}$	1.035	0.893
$e_{\sigma_{L_1}}$	0.0371	0.0439
$e_{\sigma_{L_2}}$	0.348	0.298

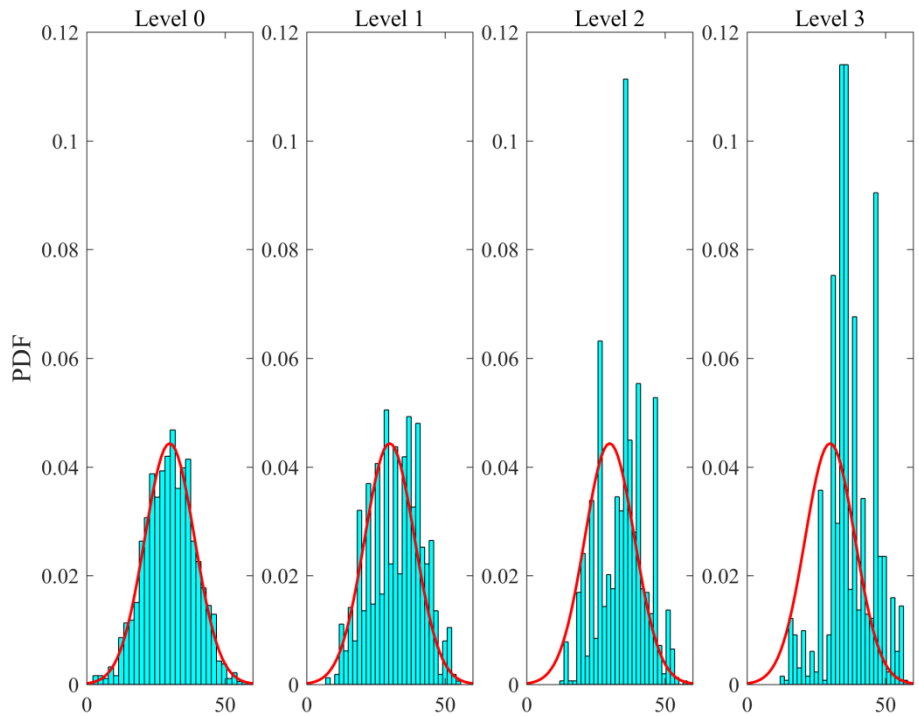
566

567 where N_{θ} is the dimension of θ . Thus when $q(\theta_l|F)$ is similar to $q(\theta_l)$, it is deduced
568 that $P(F|\theta_l) \approx P(F)$, so that the failure probability is insensitive to θ_l . Hence, by
569 comparing the conditional PDF $q(\theta_l|F)$ with the unconditional PDF $q(\theta_l)$, one can
570 obtain an indication of how much the uncertain parameter θ_l influences the system
571 failure.

572 Fig. 4 shows histograms of the conditional samples of the uncertain parameters L_1
573 and L_2 at different levels for a single SS run. It is noticed that the conditional PDFs of
574 the uncertain parameters are obviously too large for certain values. This is because there
575 are inevitably some repeated samples during the MCMC procedure. Despite some peaks,
576 it is seen that the conditional PDFs of L_1 are almost symmetric about the mean value of
577 L_1 at different levels, while those of L_2 are not symmetric and have a significant
578 rightward shift, especially at the final level. From the comparison of the shapes of the
579 conditional PDFs, it is concluded qualitatively that L_2 contributes more to the failure



(a) L_1



(b) L_2

Fig. 4. Empirical conditional PDFs of L_1 and L_2 at different conditional levels

(histograms) compared to their unconditional PDFs (solid lines)

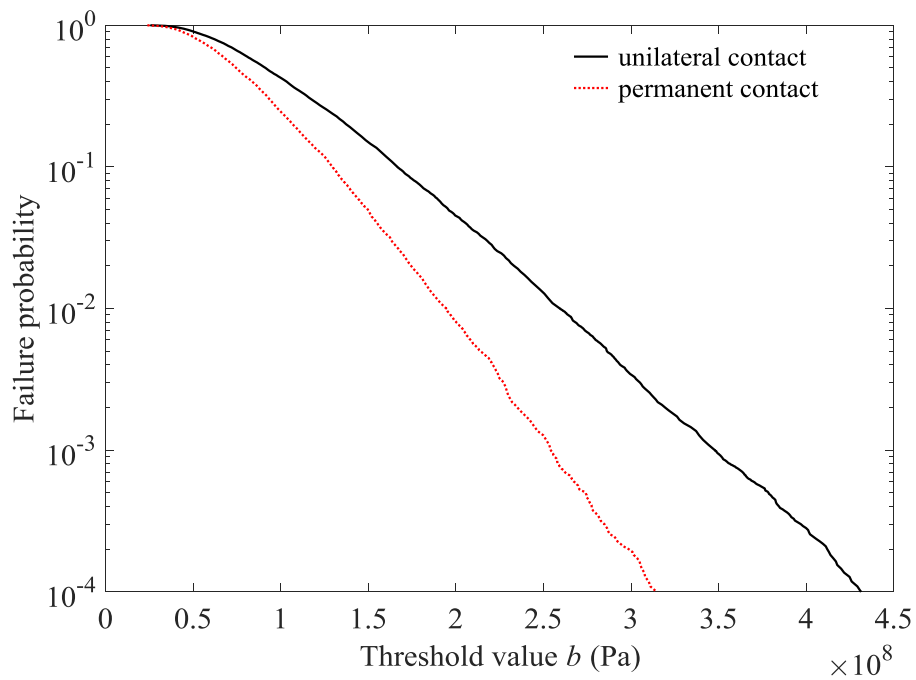
586 of subsea pipelines than L_1 . This is in agreement with the conclusion of the parametric
587 sensitivity analysis above.

588 **5.4 Study of three typical cases**

589 To study the influences of more parameters or effects on the failure of subsea
590 pipelines, three typical cases are considered.

591 **Case 1: *Unilateral contact model and permanent contact model***

592 As pointed out in the introduction, the separation of pipelines and the seabed is not
593 considered in the dynamic analysis in some literature [5, 6]. This pipeline-seabed model
594 is called a “permanent contact model”, while the model used in this paper is called a
595 “unilateral contact model”. In order to investigate the influence of the unilateral contact
596 effect on the reliability of subsea pipelines, failure probabilities of the unilateral and
597 permanent models are calculated by SS and results are shown and compared in Fig. 5. It
598 is seen that the failure probability of the permanent contact model is smaller than that of
599 the unilateral contact model at the same threshold value, so that the permanent contact
600 model is a more dangerous model in the earthquake design of subsea pipelines. The
601 comparison also shows the necessity of the consideration of the unilateral contact effect
602 in the earthquake reliability analysis of subsea pipelines.

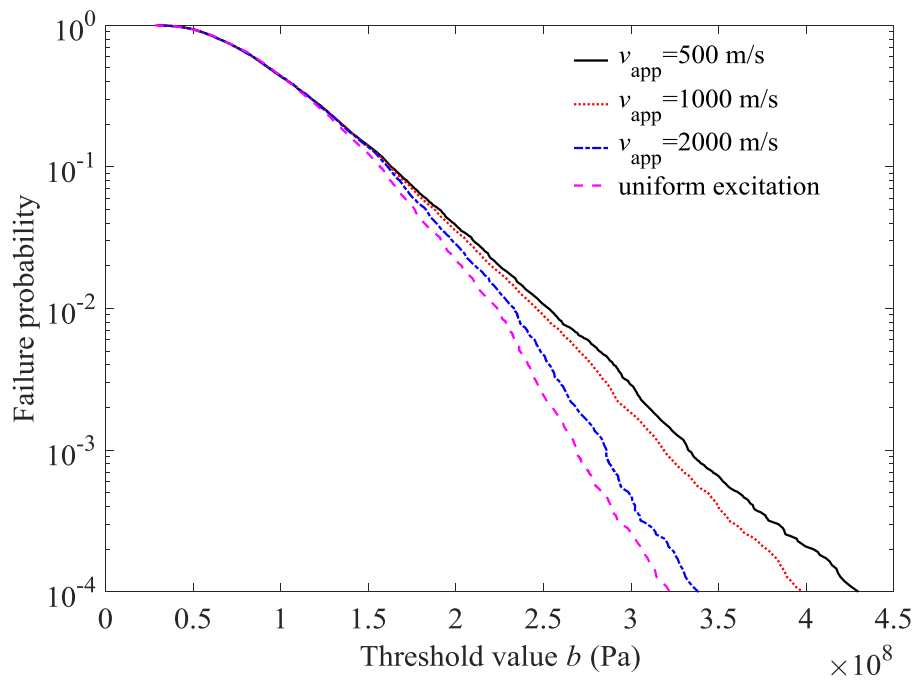


603

604 **Fig. 5.** Failure probabilities of subsea pipelines using unilateral and permanent contact
 605 models

606 **Case 2: Different apparent velocity**

607 As expressed in Eqs. (12) and (13), the apparent velocity of the earthquake waves v_{app}
 608 is one of the most important parameters affecting the spatial variation of the ground
 609 motion. The spatial variation decreases with increasing v_{app} . When v_{app} approaches
 610 infinity, the spatial variation of the ground motion vanishes and the earthquake is reduced
 611 to a uniform excitation. To study the influences of the spatial variation of the ground
 612 motion on the reliability, four cases with different v_{app} are considered, namely $v_{app} =$
 613 500 m/s, 1000 m/s, 2000 m/s and uniform excitation, as shown in Fig. 6. It is
 614 observed that the influence of v_{app} on failure is not significant in the region with relative
 615 large failure probability. But when the failure probability is at a small level, it increases



616

617 **Fig. 6.** Failure probabilities of subsea pipeline with different apparent velocity v_{app}

618

619 with decreasing apparent velocity v_{app} .

620 **Case 3: With and without free span**

621 In subsection 5.3, sensitivities of the failure probability of pipelines with respect to the

622 location and length of the free span were studied. To study further the influence of the

623 free span itself on the failure of subsea pipelines, three different cases are considered, i.e.,

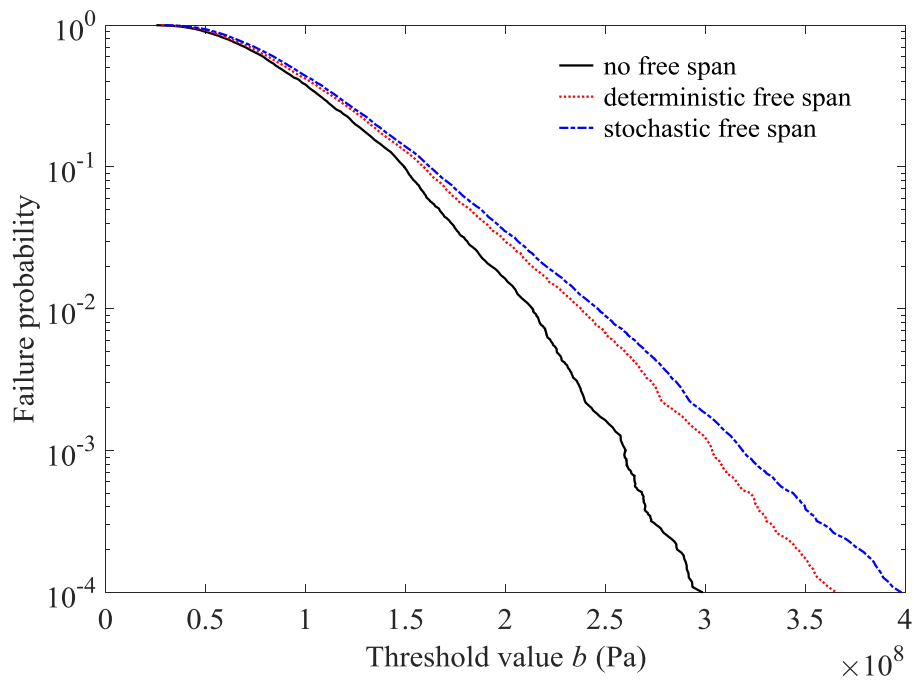
624 (1) without free span, (2) with a deterministic free span at location $L_1 = 50\text{m}$ with

625 length $L_2 = 30\text{m}$ and (3) with the uncertain free span used in subsection 5.3. The results

626 are given in Fig. 7. It is shown that the free span has significant influence on the reliability

627 of the subsea pipeline. Neglect of the free span or its uncertainty in the earthquake

628 reliability analysis will lead to an underestimate of the failure probability.



629

630 **Fig. 7.** Failure probabilities of subsea pipeline with different types of free span

631

632 **6 Conclusions**

633 In this paper, a computational framework based on subset simulation (SS) is
 634 proposed for the reliability analysis of subsea pipelines subjected to a random earthquake
 635 with spatial variation. Firstly, a mathematical model of subsea pipelines under random
 636 earthquake is established with consideration of the unilateral contact effect between the
 637 pipeline and the seabed. Then, by using the finite element method and Newmark
 638 integration method, the governing equation is discretized and the dynamic contact
 639 problem is derived as a linear complementarity problem. Finally, SS is applied for
 640 estimating the failure probability of subsea pipelines. SS expresses a small failure
 641 probability as a product of a sequence of large conditional probabilities, and provides the

642 potential to reduce the number of samples required in estimating small failure probability.

643 In numerical examples, direct Monte Carlo simulation (DMCS) is used to validate
644 the feasibility of SS in the earthquake reliability problem. It is found that the failure
645 probabilities calculated by SS agree well with those from DMCS, while the efficiency of
646 SS, as indicated by the smaller number of samples, is much greater than that of DMCS.
647 A coefficient of variation analysis shows that SS is more robust in small failure
648 probability estimation than DMCS. Results from a sensitivity analysis indicate that the
649 free span length is more influential on the failure of subsea pipelines than the free span
650 location. Three typical cases with different parameters or effects are studied. It is shown
651 that the unilateral contact effect between the seabed and pipelines, the spatial variation of
652 the ground motion and the uncertainty of the free span have great influence on the failure
653 of seabed pipelines and should be considered in earthquake reliability analysis.

654

655 **Acknowledgments**

656 The authors are grateful for support under grants from the National Basic Research
657 Program of China (2014CB046803), the National Science Foundation of China
658 (11672060), and the Cardiff University Advanced Chinese Engineering Centre.

659

660

661 **References**

- 662 [1] Teixeira AP, Guedes Soares C, Netto TA, Estefen SF. Reliability of pipelines with
663 corrosion defects. *Int J Press Vessels Pip* 2008; 85(4): 228-237.
- 664 [2] Elostá H, Huang S, Incecik A. Wave loading fatigue reliability and uncertainty
665 analyses for geotechnical pipeline models. *Ships Offshore Struct* 2014; 9(4): 450-
666 463.
- 667 [3] Elsayed T, Leheta H, Yehya A. Reliability of subsea pipelines against lateral
668 instability. *Ships Offshore Struct* 2012; 7(2): 229-236.
- 669 [4] Det Norsk Veritas. Submarine Pipeline Systems. DNV-OS-F101, 2007.
- 670 [5] Lin YK, Zhang R, Yong Y. Multiply supported pipeline under seismic wave
671 excitations. *J Eng Mech* 1990; 116(5): 1094-1108.
- 672 [6] Soliman HO, Datta TK. Response of overground pipelines to random ground motion.
673 *Eng Struct* 1996; 18(7): 537-545.
- 674 [7] Xu T, Lauridsen B, Bai Y. Wave-induced fatigue of multi-span pipelines. *Mar Struct*
675 1999; 12(2): 83-106.
- 676 [8] Sollund HA, Vedeld K, Fyrileiv O. Modal response of short pipeline spans on partial
677 elastic foundations. *Ocean Eng* 2015; 105: 217-230.
- 678 [9] Maier G, Andreuzzi F, Giannessi F, Jurina L, Taddei F. Unilateral contact,
679 elastoplasticity and complementarity with reference to offshore pipeline design.
680 *Comput Methods Appl Mech Eng* 1979; 17-18: 469-495.

- 681 [10]Kalliontzis C, Andrianis E, Spyropoulos K, Doikas S. Finite element stress analysis
682 of unilaterally supported submarine pipelines. *Comput Struct* 1996; 61(6): 1207-
683 1226.
- 684 [11]Baniotopoulos CC. Optimal control of submarine cables in unilateral contact with
685 the sea-bed profile. *Comput Struct* 1989; 33(2): 601-608.
- 686 [12]Panagiotopoulos P D. *Inequality Problems in Mechanics and Applications: Convex*
687 *and Nonconvex Energy Functions*. Birkhauser, Boston, 1985.
- 688 [13]Der Kiureghian A. A coherency model for spatially varying ground motions. *Earthq*
689 *Eng Struct Dyn* 1996; 25(1): 99-111.
- 690 [14]Lin J H. A fast CQC algorithm of PSD matrices for random seismic responses.
691 *Comput Struct* 1992; 44(3): 683-687.
- 692 [15]Der Kiureghian A, Neuenhofer A. Response spectrum method for multi-support
693 seismic excitations. *Earthq Eng Struct Dyn* 1992; 21(8): 713-740.
- 694 [16]Heredia-Zavoni E, Vanmarcke EH. Seismic random-vibration analysis of
695 multisupport-structural systems. *J Eng Mech* 1994; 120(5): 1107-1128.
- 696 [17]Shinozuka M. Monte Carlo solution of structural dynamics. *Comput Struct* 1972;
697 2(5-6): 855-874.
- 698 [18]Hohenbichler M, Rackwitz R. First-order concepts in system reliability. *Struct Saf*
699 1982; 1(3): 177-188.
- 700 [19]Der Kiureghian A, Lin HZ, Hwang SJ. Second-order reliability approximations. *J*

701 Eng Mech 1987; 113(8): 1208-1225.

702 [20]Hong HP. An efficient point estimate method for probabilistic analysis. Reliab Eng
703 Syst Saf 1998; 59(3): 261-267.

704 [21]Melchers RE. Importance sampling in structural systems. Struct Saf 1989; 6(1): 3-
705 10.

706 [22]Engelund S, Rackwitz R. A benchmark study on importance sampling techniques in
707 structural reliability. Struct Saf 1993; 12(4): 255-276.

708 [23]Au SK, Beck JL. Estimation of small failure probabilities in high dimensions by
709 subset simulation. Probabilist Eng Mech 2001; 16(4): 263-277.

710 [24]Au SK, Ching J, Beck JL. Application of subset simulation methods to reliability
711 benchmark problems. Struct Saf 2007; 29(3): 183-193.

712 [25]Tee KF, Khan LR, Li HS. Application of subset simulation in reliability estimation
713 of underground pipelines. Reliab Eng Syst Saf 2014; 130: 125-131.

714 [26]Yuan J, Allegri G, Scarpa F, Rajasekaran R, Patsias S. Probabilistic dynamics of
715 mistuned bladed disc systems using Subset Simulation. J Sound Vib 2015; 350: 185-
716 198.

717 [27]Cadini F, Avram D, Pedroni N, Zio E. Subset Simulation of a reliability model for
718 radioactive waste repository performance assessment. Reliab Eng Syst Saf 2012;
719 100: 75-83.

720 [28]Vahdatirad MJ, Andersen LV, Ibsen LB, Sørensen JD. Stochastic dynamic stiffness

721 of a surface footing for offshore wind turbines: Implementing a subset simulation
722 method to estimate rare events. *Soil Dyn Earthq Eng* 2014; 65: 89-101.

723 [29] Au SK, Beck JL. Subset simulation and its application to probabilistic seismic
724 performance assessment. *J Eng Mech* 2003; 129(8): 901-917.

725 [30] Paidoussis MP, Laithier BE. Dynamics of Timoshenko beams conveying fluid. *J*
726 *Mech Eng Sci* 1976; 18(4): 210-220.

727 [31] Morison JR, Johnson JW, Schaaf SA. The force exerted by surface waves on piles. *J*
728 *Petrol Technol* 1950; 2(5): 149-154.

729 [32] Loh CH, Yeh YT. Spatial variation and stochastic modelling of seismic differential
730 ground movement. *Earthq Eng and Struct Dyn* 1988; 16(4): 583-596.

731 [33] Clough R W, Penzien J. *Dynamics of Structures*. New York: McGraw-Hill, 1993.

732 [34] Samaras E, Shinzuka M, Tsurui A. ARMA representation of random processes. *J Eng*
733 *Mech* 1985; 111(3): 449-461.

734 [35] Berg GV, Housner GW. Integrated velocity and displacement of strong earthquake
735 ground motion. *B Seismol Soc Am* 1961; 51(2): 175-189.

736 [36] Jensen HA, Mayorga F, Valdebenito MA. Reliability sensitivity estimation of
737 nonlinear structural systems under stochastic excitation: A simulation-based
738 approach. *Comput Methods Appl Mech Eng* 2015; 289: 1-23.

739 [37] Arifin RB, Yusof WM, Zhao PF, Bai Y. Seismic analysis for the subsea pipeline
740 system. In: *Proceedings of the ASME 2010 29th International Conference on Ocean,*

741 Offshore and Arctic Engineering, OMAE2010-20671, Shanghai, China, 2010.

742 [38]Dumanogluid AA, Soyluk K. A stochastic analysis of long span structures subjected

743 to spatially varying ground motions including the site-response effect. Eng Struct

744 2003; 25(10): 1301-1310.